Proceedings of 9th-WMM2020- Rome, November 2020, ISBN978-88-900033-1-8, pp117-135

# Metallurgical Model of HTCA for GO Silicon Steel with prevision of Magnetic Properties (B800) and Secondary Grain Size (MOGOCA-EVO)

Giuseppe Carlo Abbruzzese, Spires srl, Terni, Italy

## 1. Introduction and scope

The availability of a Simulation Tool capable of describing the basic processes and microstructure evolution during the High Temperature Coil Annealing (HTCA) of GO Electrical Steel remains, and has been, for many years, a very urgent need for the relevant Industrial and Scientific Community.

However, due to the enormous complexity of the phenomena involved and the high number of relevant technical parameters influencing the final results, such technology has always been confined in an area where only the continuous experience gained on the ground, a trials and errors approach or a set of complex laboratory experiments were the only means for reaching a stable production and/or designing new process or product.

An attempt to create a Mathematical Tool (MOGOCA) has already been presented and discussed in a previous paper [1].

The tool was built to investigate in detail the kinetics of the stability of grain growth inhibitors (second phase particles : nitrides ) as well as evaluating the oxidation kinetics of Aluminum on the strip surface and its effects on precipitate stability and Glass Film formation.

In the present paper, an important step has been executed by introducing a Secondary Recrystallization (SRX) module, which is capable, considering microstructure and texture in the primary recrystallized stage (grain size, grain heterogeneity, texture ), of treating the whole microstructure evolution in HTCA and to predict the final magnetic properties (B800) and the secondary grain size (MOGOCA-EVO).

With such a comprehensive tool it is thus possible to perform, in an integrated way, a sensitivity analysis of the final magnetic results as a function of all the processes and technical parameters relevant for HTCA process: Al,N,Si, N Injected, Total Oxygen, Strip Thickness, Width, Type of Oxide layer, MgO porosity, LOI(% $H_2O$ in MgO), MgO weight on strip surface, process gas MIX ($H_2$, $N_2$, d.p.), gas mass flow, coil weight, hood geometry, Thermal Cycle and changes of gas mix, etc. Such analysis can be also performed as a function of the process and metallurgical upstream parameters responsible for primary grain size, grain size heterogeneity and texture (namely: the Inherent Inhibition , full Chemical Composition, T-slab annealing, Hot Rolling and APL

conditions, carbides and carbon in solution, % of Cold Rolling, T of WR, URA, Decarb. Thermal Cycle, etc..).
Moreover, its robust scientific foundation, its design as a practical engineering tool and its capability of clarifying the interplay of such large number of parameters, make of MOGOCA-EVO the natural candidate to become an invaluable tool for technicians/experts involved in Production stabilization, Quality Improvement and Research for new Process and Products.

# 2. Background of MOGOCA and outline of MOGOCA-EVO

It is well known that an optimal secondary recrystallization (SRX) process in Grain oriented electrical steel requires the presence of grain growth inhibitors (mainly Aluminum Nitrides for the High-Grade material (HGO)). These reduce the driving force of continuous grain growth during the HTCA treatment, allowing the selection of Goss grains among the various texture components present in the grain matrix. The extremely low concentration of Goss grains in the primary recrystallized microstructure and the relative rarity of those capable of selectively growing are responsible for the large secondary grain size, typical of HGO electrical steel. The final magnetic properties, including secondary grain size effect, are therefore significantly modulated by the way grain growth inhibitors lose their restraining force (by particle dissolution or Ostwald ripening process) along the thermal cycle. Being the Inhibition strength $I_Z$ well characterized by the following formula

$$I_z = \frac{6}{\pi}\,\frac{f_v}{r}$$

Where $f_v$ = volume fraction of precipitates and $r$ = average size of the particles

it turns out that both the parameters $f_v$ and $r$ (volume fraction and mean radius) are affected by the thermal treatment, the first mainly by dissolution of precipitates while the second mainly by Ostwald ripening. They both also cause a reduction in $I_Z$ albeit following different physical paths (fig.1a,1b).

Moreover, the drop of Inhibition strength at high temperature is also a heterogeneous process along the strip thickness, due to the unavoidable oxidation of Aluminum on the strip surface where less thermodynamically stable oxides are present ($SiO_2$, $Fe_2SiO_4$ as opposed to $Al_2O_3$). The dissolution of the precipitates, with the associated increase of Aluminum in solution, creates a gradient of inhibitors, continuously expanding and invading the inner zones of the strip (fig2a-2d).

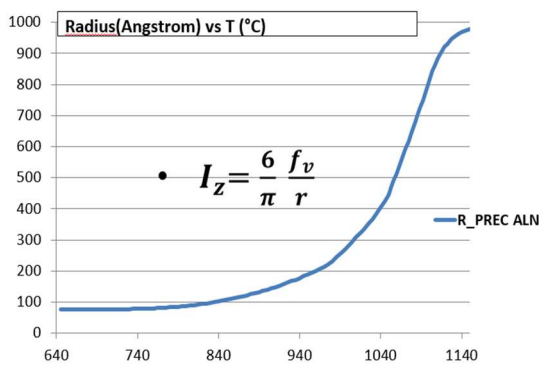


Fig. 1a Example of evolution of ALN particle size in HTCA

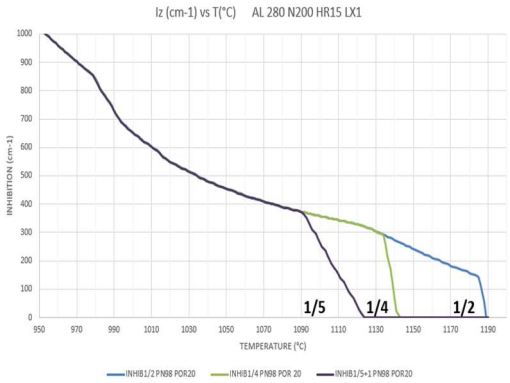


Fig.1b Example of Inhibition decay at various sheet thickness depths

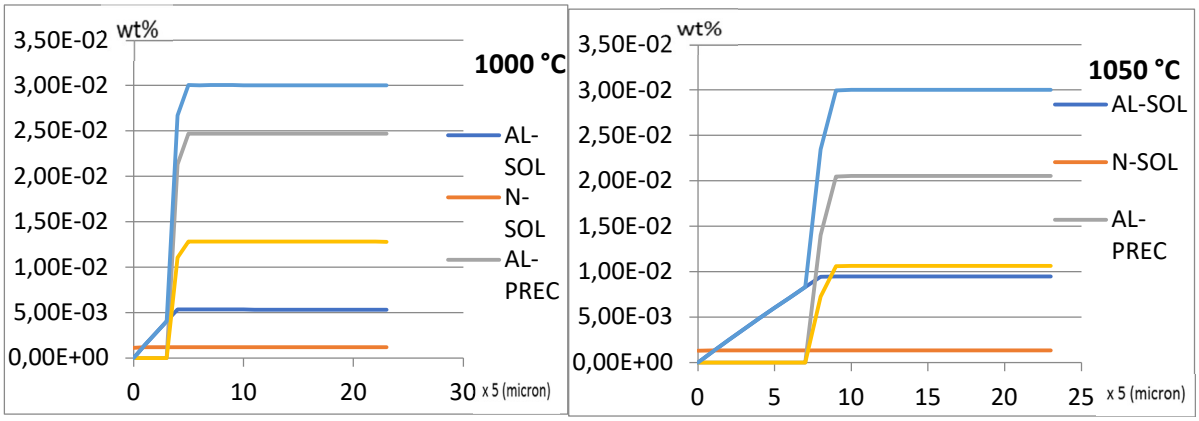


Fig.2a and 2b: examples of evolution, through thickness (0,23mm), of Aluminum, total and in solution, N in solution, and ALN, at different temperatures during HTCA

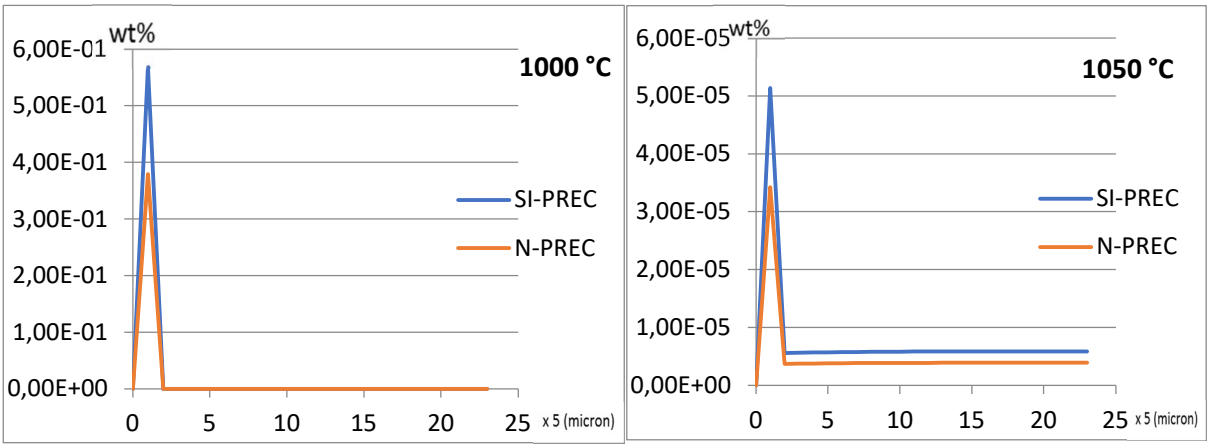


Fig.2c and 2d: example of evolution of $Si_3N_4$, at different temperatures during HTCA

The consequent creation of a depleted zone of ALN precipitates, produces a favorable condition for the precipitation of $Si_3N_4$ near the surface, which competes with ALN for Nitrogen, creating, according to the specific conditions, further perturbation on Aluminum nitrides stability, even in the deeper layers along the thickness of the strip. Such perturbation persist until Silicon Nitrides are completely dissolved (due to their relatively lower thermodynamic stability in respect to ALN); this phenomenon can be further modulated by the kinetics of atomic Nitrogen extraction-penetration in the steel, as a function of the presence of Nitrogen in the gas mix and of its diffusion kinetics in the inter-spire gap [1].

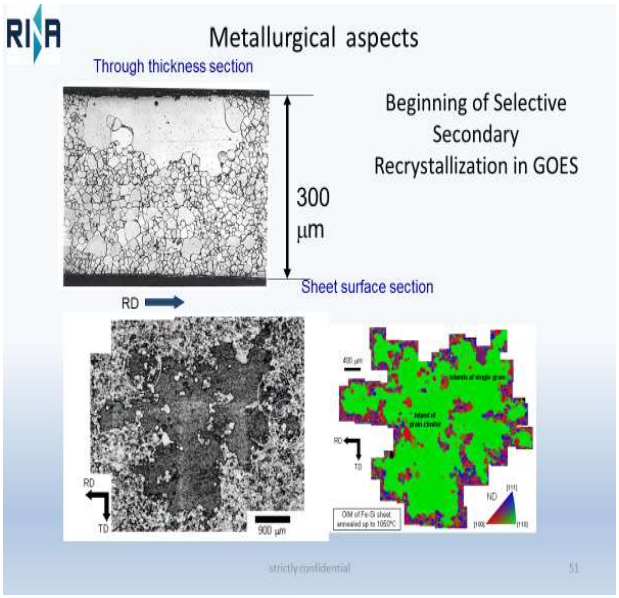


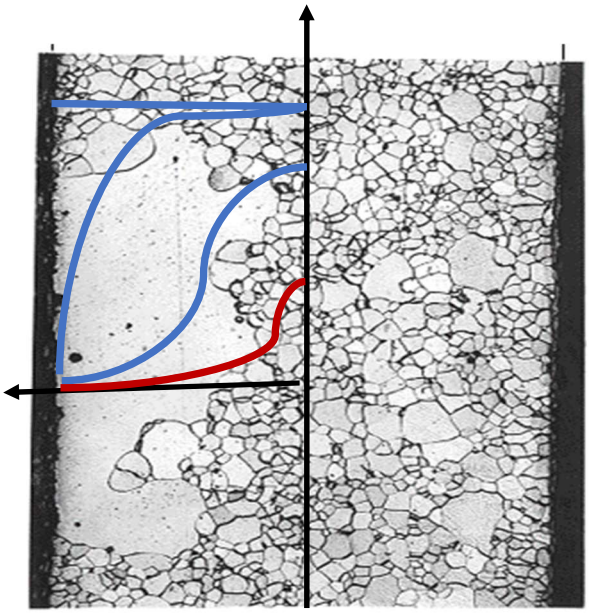

Fig.3a example of secondary Goss grains Fig.3b Schematic of Inhibition gradient

Such gradient of inhibitors is also responsible of the early nucleation of Goss grains at a certain distance from the surface (1/5-1/4 of the strip thickness). This nucleation zone exists due to the presence of a favorable texture condition produced by the previous hot and cold rolling processes (deformation path including the effect of friction forces operating for an extent between 1/6 to 1/4 of the total strip thickness).

## 3. Comparison of MOGOCA predictions with experiments

A detailed investigation of interrupted HTCA experiments is reported in Fig4a. The main parameters adopted are: Low Slab Reheating Temperature (LSRT) technology, Heating Rate 15°C/h, Al 280 ppm, N190 ppm, standard procedure for the rest. The experiments aimed at measuring the evolution of Total Aluminum, Total Nitrogen and Nitrogen as ALN along the whole HTCA cycle. Increasing the temperature, the transformation of $Si_3N_4$ in ALN increases up to a maximum [1]. ALN then starts to decrease near the surface and gradually towards the middle of the strip due to particle dissolution (here the measurement of the total ALN averages these processes). The evolution of Total Aluminum and Total Nitrogen, at high temperature, shows the same tendency. What is worth noticing is a “rate discontinuity” in the dissolution of ALN at

temperatures around 1000°C which at first glance does not seem to correspond to any specific effect.

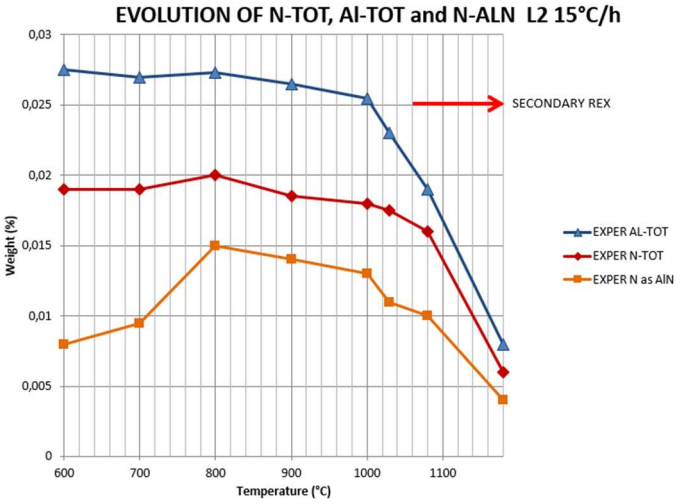


Fig.4a

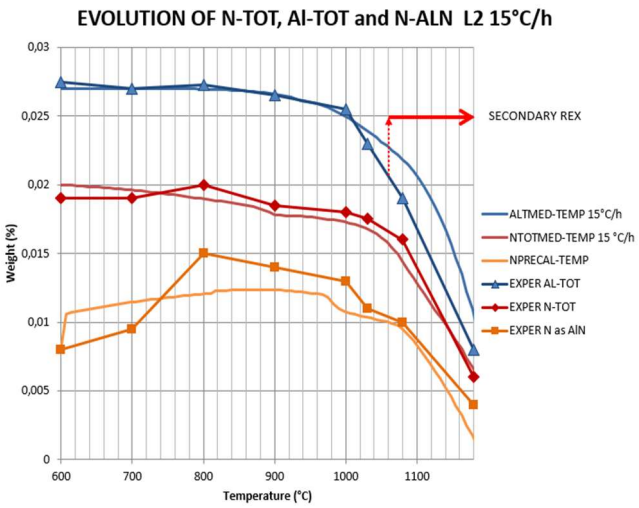


Fig.4b

In Fig.4b, with the aid of experiments simulated with identical process conditions through MOGOCA Software, one can notice that the transformation of Silicon Nitrides into ALN seems to happen slightly earlier than the measured data suggest (based on the fact that in the MOGOCA code it is assumed that nucleation of precipitates starts on preexisting defects/particles so the activation energy for precipitation is considered rather low). It is possible to see that total Aluminum and Nitrogen evolution are substantially the same. Take notice of how the “rate of discontinuity”, a remarkably unique feature of the dissolution curve of Aluminum Nitrides in the SRX zone (above 950°C), is correctly reproduced. The reason for such an effect is observable in Fig4.c where, thanks to MOGOCA, we can also see the evolution of Silicon Nitrides (Nitrogen as $Si_3N_4$): these show a continuous dissolution, in favor of the precipitation of the most stable ALN. However, due to the concurrent dissolution of ALN, after reaching a certain temperature Silicon Nitrides have a precipitation peak, creating a perturbation in the stability of ALN (see also fig.2a-2d). Such interaction is at the basis of many typical features of ALN Inhibition drop (e.g. see fig1b the evolution kinetics of Iz at T above 980°C) and it is modulated by many process and metallurgical parameters ($N_2$ in gas mix, surface oxide structure, N injected, Silicon and Aluminum content, heating rate,…..)

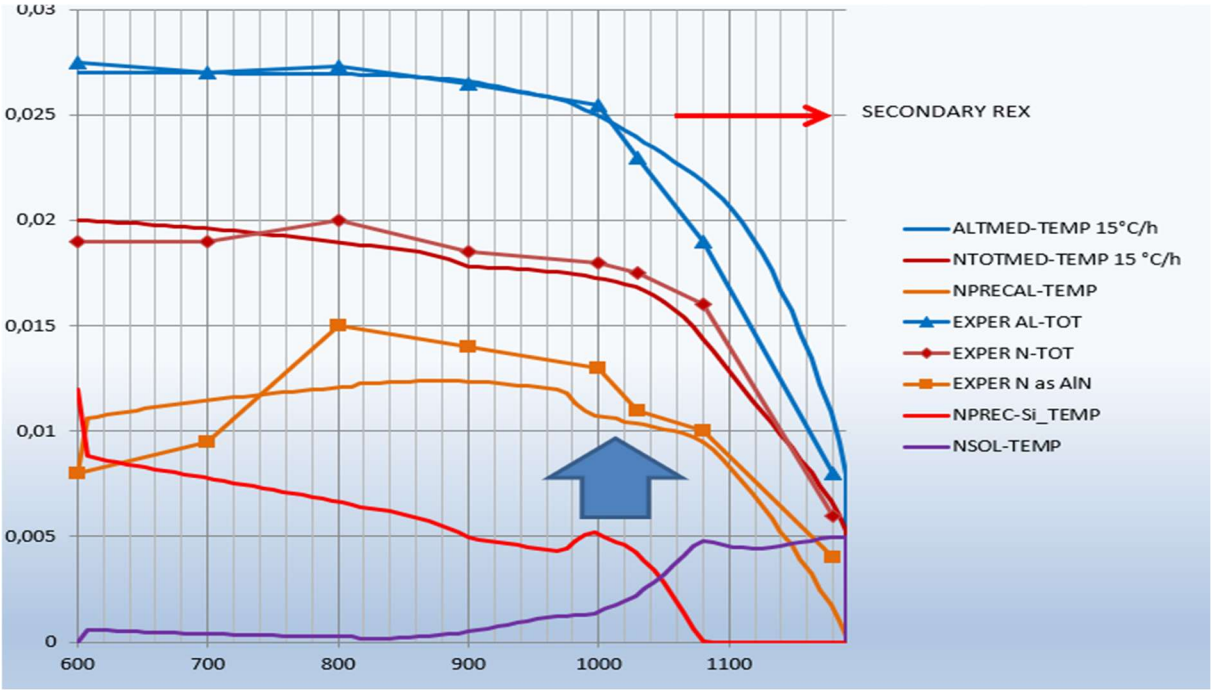


Fig.4c Experiments in comparison with MOGOCA prediction (macroscopic effect of Silicon nitrides precipitation on Aluminum Nitrides stability)

## 4. Basics for Goss Grain selection

The fact that Goss grains (with a certain angular spread around the exact crystallographic position (110)< 001>) are the only grains which are selected during secondary recrystallization, set the Scientific Community on a quest to find the possible physical mechanism allowing for such phenomena. Even nowadays there is still debate among various researchers on the topic.

However, many years of experimental evidence led to the following conclusions:

- Goss grains do not have in general size advantage in the primary recrystallized microstructure [3]
- There is no other essential mechanism, beside grain growth and the presence of a restraining force (Grain Growth inhibitors), allowing the onset of secondary recrystallization [3,6,7]
- Texture selection is induced by some differences in boundary energy (and/or mobility) which Goss grains experience during the growth process, due to their special conditions of: 1) being an *extremely scarce texture component* [3-5] embedded in a primary recrystallized texture formed by a few other majority texture components, 2) having some special orientation relationship with at least one of them [6]

The condition of a special orientation relationship (for instance based on CSL model) can theoretically lead to the measurement of a different growth rate ,which makes it difficult to discriminate if it is the boundary energy or the boundary mobility to be affected by such special relationship, as they both are a factor in the growth rate equation [7,8].

However, besides the old paper of Ibe -Lucke, which emphasizes the role of 27° rotation around <110> axes (also CSL 19b ) in producing higher growth rate on the BCC structure [9] , there is a lot of experimental evidence pointing out an higher frequency of CSL boundary in the microstructure for Goss grains [10-16].

On the other hand a CSL boundary is well known to be a site of relatively lower boundary energy (see experimental in fig.5 for a tilt boundary).

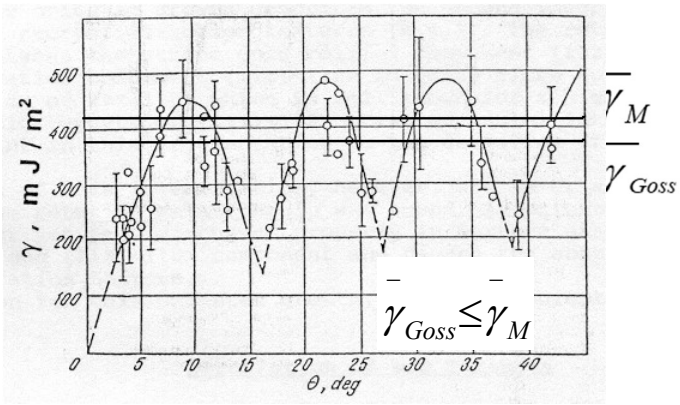


*Avramov Y.S. et al., Phys. of Metals, 36, (1973), p.198.*

Fig.5 Measured energies for tilt boundaries

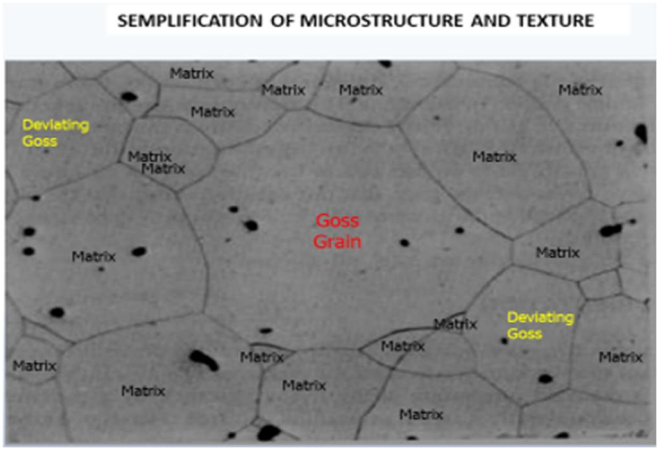


Fig.6 High number of favorable boundaries for a minority texture

Therefore, in presence of the basic condition that Goss texture component is a minority texture component in the microstructure [ 4-6], paired with the high frequency of CSL boundary for Goss grains with one or more majority texture components (matrix grains), one can assume configurations as shown in fig.6, should be easily established.
Such a situation will statistically lead to a higher number of CSL boundaries active for Goss grains, with a relatively lower average boundary energy for the growth (see fig.5). Furthermore, the restraining force of the particles will be less effective with a low average energy boundary than with a high energy one thus allowing an even more effective growth advantage for Goss grains [6-8].

# 5. MOGOCA-EVO outline

Several years have been passed since the development of a Statistical Theory of Grain Growth, which is able to describe grain growth in the presence of texture and drag effects [ 2,4-7]. However due to the lack of knowledge about how the Inhibition parameter Iz evolved in real conditions and how it was connected to many relevant process and metallurgical parameters operating during HTCA treatment, the main use of the aforementioned theory has been that of testing the basic mechanisms and deriving qualitative or semiquantitative predictions about the influence of the most relevant metallurgical parameters (grain size distribution, texture, inhibition drop, etc..) [6,7]. Moreover, when taking into account the full set of grain size distributions (Fig.7) and the associated continuity equations, it very often lead to very long computation time per simulation, making it not very useful for practical and industrial scope.

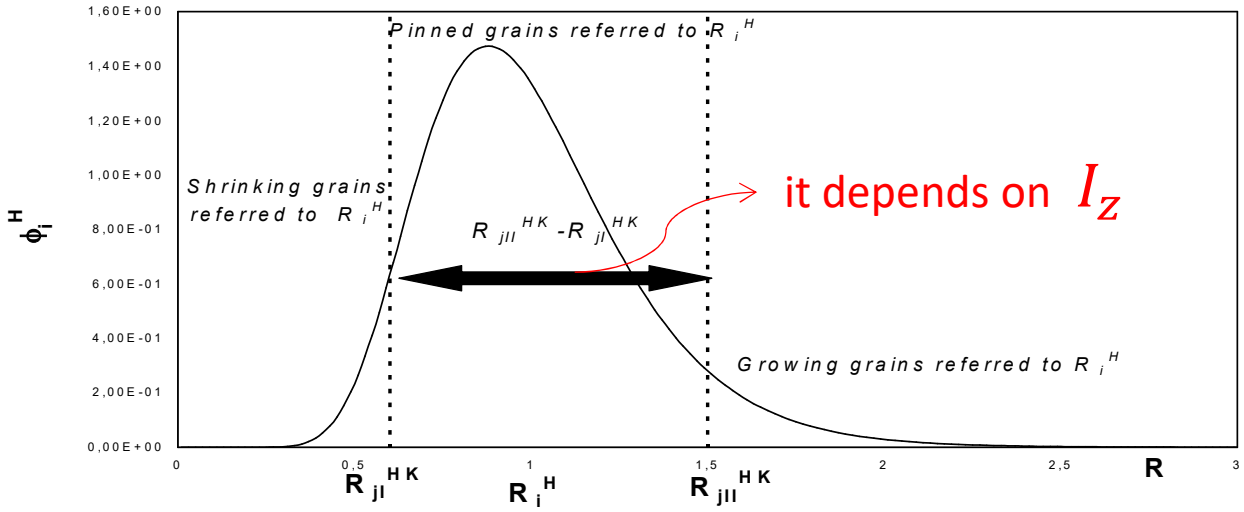


Fig.7. effect of Inhibition intensity Iz on the dynamical “pinned” grain size zone. The parameter Iz influences such intervals independently for any texture components and appears in the basic equations as a critical term for the Grain size distributions evolution

$$\frac{dR_i^H}{dt} = \sum_{j=1}^{j_I^{HK}} \sum_{K=1}^{N_t} \frac{\phi_j^k R_j^2 m^{HK}}{\phi_j^k R_j^2} \cdot \left( \frac{\gamma^K}{R_j} - \frac{\gamma^H}{R_i} + \gamma^{HK} I_Z \right) + \sum_{j=1}^{j_{II}^{HK}} \sum_{K=1}^{N_t} \frac{\phi_j^k R_j^2 m^{HK}}{\phi_j^k R_j^2} \cdot \left( \frac{\gamma^K}{R_j} - \frac{\gamma^H}{R_i} - \gamma^{HK} I_Z \right).$$

Nowadays, thanks to MOGOCA software, it is possible to reconsider the approach, having now full control over the evolution of grain growth inhibition along the sheet thickness and during the entirety of treatment time. Therefore, it can be also possible to simplify the grain size microstructure and texture to grasp the main relevant parameters and information without losing the required precision in grain growth and texture evolution prediction.

A simplified microstructure has thus been designed (Fig.8), in which a texture made only of grains representing Goss and deviating Goss (Goss grains which deviate from the exact crystallographic position by just a few degrees) is embedded in a texture of so called “matrix” grains. The grain size distribution is broken down in two classes: one representing the larger grains (typically 2-3 times the size of average grains) where Goss, deviating Goss and Matrix grains are present with their specific numerical frequency, but without specific size advantage among these grains (which if necessary, can even be regulated); the other class representing the average grains, largely composed of matrix grains and very small number of Goss and deviating Goss grains. A factor given by the ratio of maximum grains and average grains is the element somehow capable of accounting for the standard deviation of the distribution ($HE=R_{max}/R_{mean}$: Grain Size heterogeneity factor).

Here, a matrix of boundary energy represents the possible kind of contacts among the grains and a difference of about 10% less energy is assumed for goss grain- matrix boundary in respect to matrix-matrix boundary (600 erg/cm2). Deviating Goss-Matrix boundary has instead about 7% less energy than the general boundary.

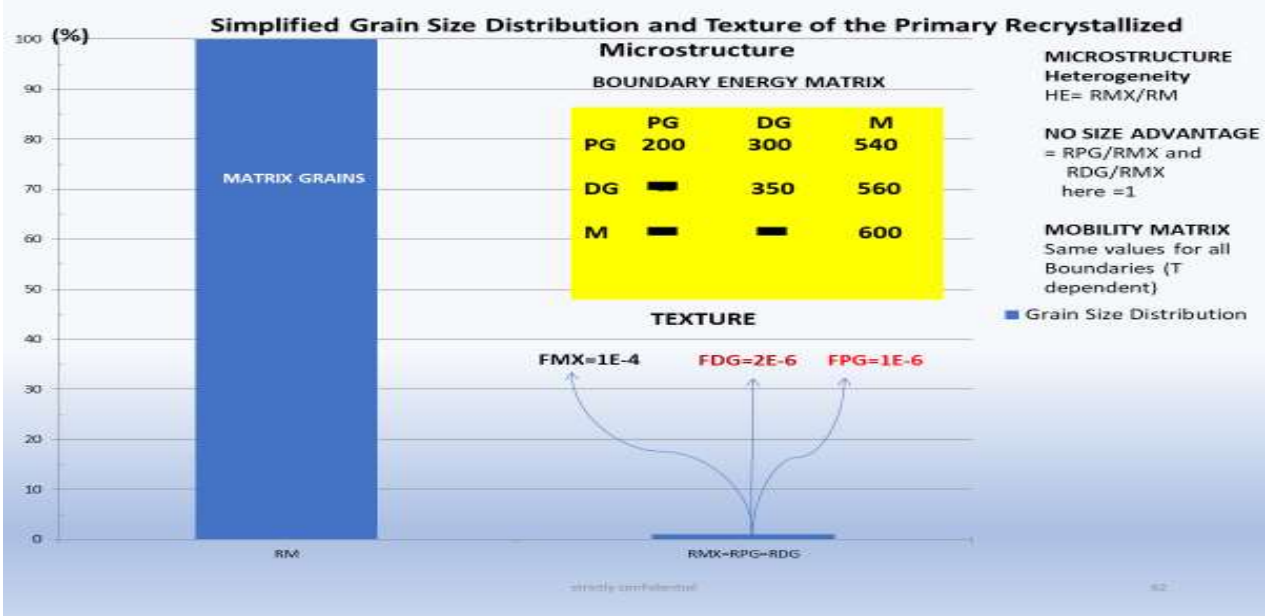


Fig.8 Simplified GS Distribution,Texture, Boundary energy an mobility matrix

For the sake of simplicity, no differentiation in the mobility matrix is assumed here. Mobility is described by a temperature dependent Arrhenius function, using experimental data from scientific and technical literature.

The evolution of the volume fraction of the various texture components (PG=precise GOSS, DG=Deviating GOSS and M=Matrix grains) dynamically represents the evolution of average B8 (magnetic induction at 800 Asp/m) which is weighted by a B8 “saturation” value for each texture component, according to the relative precision of the orientation assumed (see Fig.9).

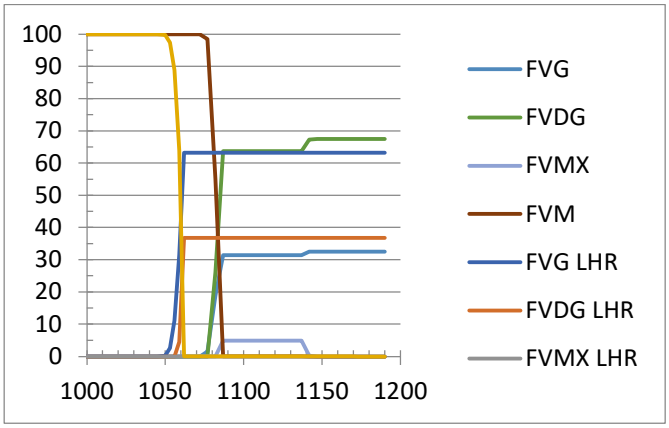


**Magnetic Induction vs Texture**

- $B8_{PG}$ = 1940 mT at Si=3.25%
- $B8_{DG}$ = 1870 mT
- $B8_{MX}$ = 1600 mT

$$B8_{av(\%Si)} = F_{VPG} * B8_{PG(\%Si)} + F_{VDG} * B8_{DG(\%Si)} + F_{VMX} * B8_{MX(\%Si)}$$

Fig.9 Example of Volume fraction kinetics for PG, DG, MX (matrix grains in the tail), and M at High and Low Heating Rate. On the right, B8 "saturation" values assumed for the Three texture components

The functional scheme of MOGOCA-EVO and the interaction with MOGOCA is represented and summarized in the next graph

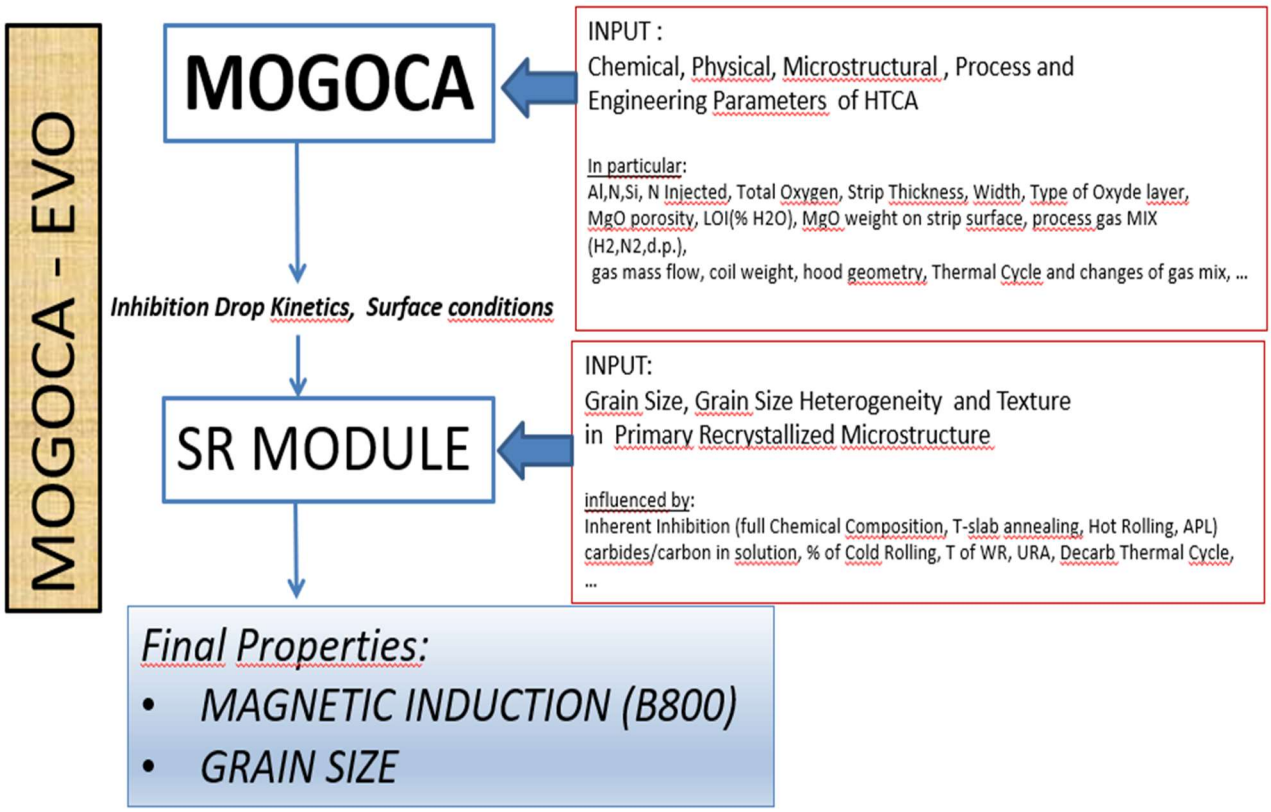

# 6. Primary Grain Size (PGS) effect vs experiments

A common experience for the experts in the field of GO electrical steel, is dealing with the instability of magnetic properties in relation to primary recrystallized microstructure (after decarburization and nitriding). A typical parameter used to characterize such microstructure is the Grain Size (usually measured by intercept method, for practical reason). The general feature always appears as in figs.10,11. As grain size increases (normally by increasing the temperature of decarburization) there is a continuous improvement of B8, up to a maximum, followed by a drastic drop of the magnetic induction even for a small increase in Grain size. The position of the abrupt discontinuity, the level of B8 reachable and the slope of increasing B8 depend on the many other variables at play (from chemical composition to all other relevant process parameters). A comparison with a simulation by MOGOCA-EVO pictured in Fig.10 shows rather similar quantitative features of the process, (even if detailed information about the process parameters adopted in the experiments were not fully available for testing better the data). Moreover, another element that is also interesting to see in the MOGOCA-EVO simulation is the effect on Secondary Grain Size (SGS) of such evolution. In fact, SGS also increases as a function of PGS, reaching a maximum and dropping in the same way as B8. It is shown that the effect of increasing PGS is connected to a more favorable Goss Grains growth selectivity, as secondary recrystallization starts at higher temperature and will match a zone of slower inhibition drop (see fig 1b, for example). In this zone more precise Goss grains, which will start to grow relatively earlier, have time to gain size advantage (therefore less and more precisely oriented Goss grains in the final microstructure). However this favorable evolution ends abruptly when the inhibition decay (at 1/5 of thickness) is strongly accelerated (by the continuous oxidation of aluminum at the expenses of surface oxides and by the associated instability of precipitates below the surface), with a depletion front moving continuously towards the inner zone (figs 2a-d) of the sheet thickness[1].

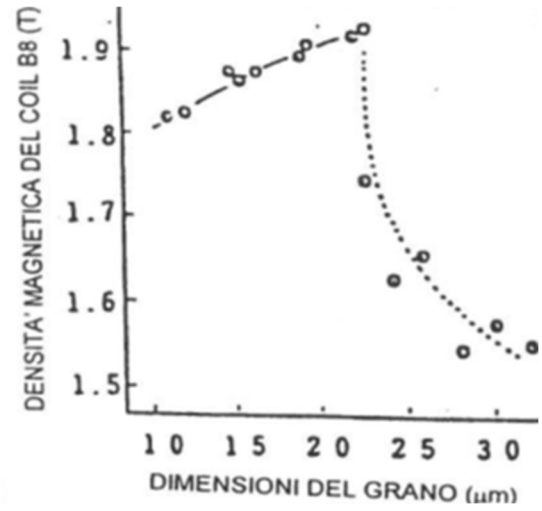


Fig.10

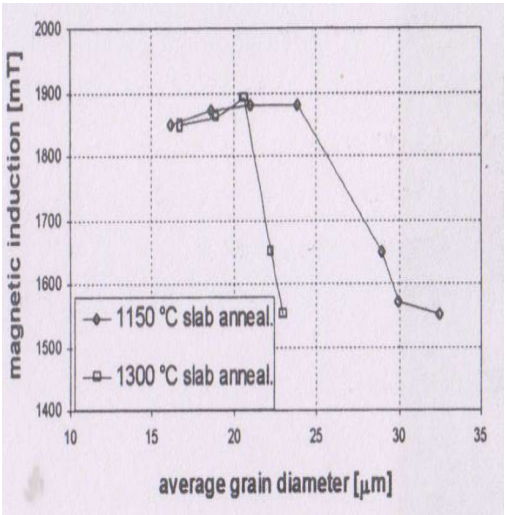


Fig.11

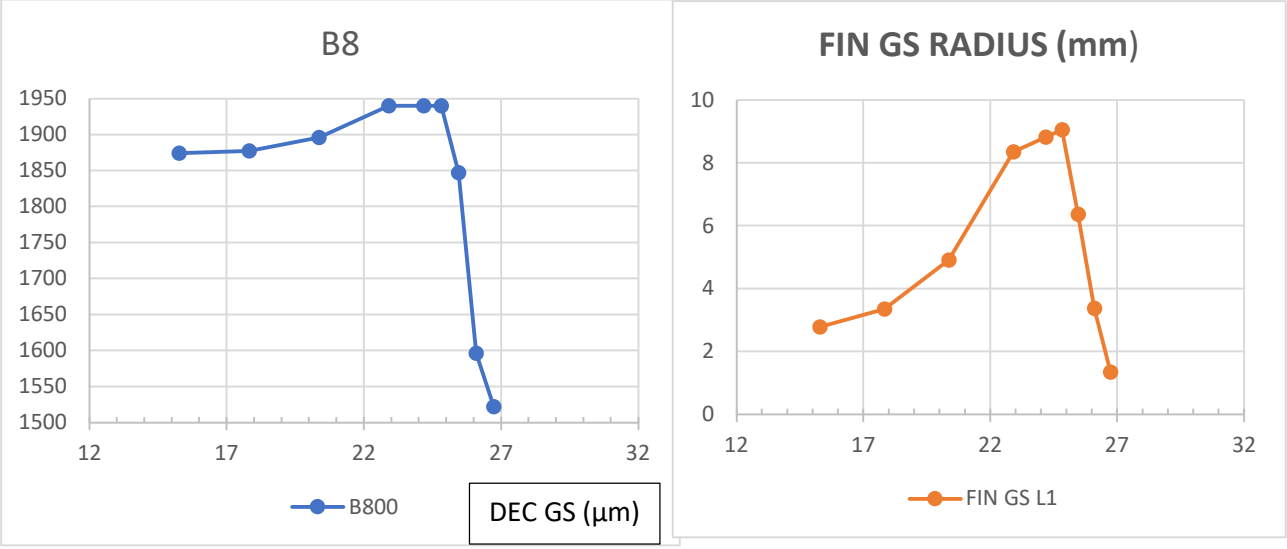


Fig 12. - Example of MOGOCA EVO Prediction (s=.30mm, Si=3,2%,Al=270ppm,N=220ppm, HR10°C/h,PN2=25%,LOI=2%,….) : B8 (mT) as a function of grain size (Intercept- µm) after Decarb
- Average Final Grain Size (Radius- mm) vs DECARB grain size (µm)

Fig.13 shows the effect of the PGS heterogeneity. The increase of the HE=$R_{max}/R_{mean}$ parameter, for the same average PGS, causes a reduction of Magnetic potential and a shift to a higher PGS at moment of the drastic drop of B8. The reason for this, on a metallurgical level, is that, by increasing HE, the starting temperature of Secondary recrystallization is shifted to a lower temperature, where the Inhibition drop tends to be higher due to interference with the precipitation of $Si_3N_4$ (see the left part of Fig. 1b for Iz). The case of Fig.11 [17], shows an instability of B8 as a function of PRGS both for LSRT and ISRT (Intermediate Slab Reheating Temperature), which is modulated, besides the effect of PGS, also by a parallel increase of HE factor and strictly induced by the inherent inhibition value present in the two cases. Details about these combined effects (PGS and PGS Heterogeneity) will be given elsewhere [18].

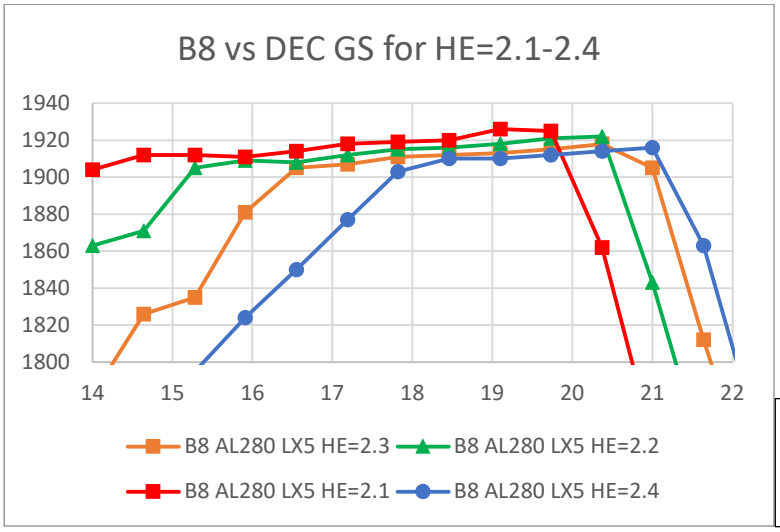


Fig.13 Example of the effect of PGS Heterogeneity HE=(Rmax/Rmean)

# 7. Effect of Nitrogen: comparison with experiments

Ever Since HiB technology was introduced, it became apparent of the importance of Nitrogen content (typically 80-90 ppm) in such GO electrical steel, to achieve optimal final properties. However, it was also clear that, in the case of High Slab Reheating Temperature (HSRT), the inherent inhibitors were mostly formed before the starting of HTCA, creating an exceptionally fine and controlled grain microstructure (8-10 micron). Nevertheless, it was also found that a limited quantity of Nitrogen in the gas mix during HTCA process was helpful to stabilize the process. In fact experiments on interrupted HTCA processes showed that HiB material was able to gain a certain amount of Nitrogen (10-30 ppm) due to the porosity of oxide layer, until an adequate glass film was formed, which would then lead to a more effective sealing of the surface. It became also clear that magnetic properties would be impaired if Nitrogen, would have exceeded the very tightly defined limit.
When the technology of LSRT with rather low inherent inhibition and nitriding at final strip thickness (so-called “acquired inhibition”) was introduced, the amount of Nitrogen in the steel after decarburization increased up to 220-260 ppm. This was now possible by exploiting the microstructure condition of having PGS in the range of 20-25 micron. In the meantime, ISRT technology (1250-1300 °C) was also introduced, as well as Thin slab technology, both with intermediate inherent inhibition (in case of Thin Slab such inhibition level is mostly due to its specific solidification microstructure and not because of the slab temperature adopted, which can be rather low). Here the typical PGS is in the range 16-20 micron with an associated optimal Nitrogen content of 180-220 ppm.
Such variety of behaviors led to a more detailed investigation of what would happen with intermediate inherent inhibitors, between HiB technology (HSRT) and those of conventional LSRT technology. Based on a previous work of Cicalè et al. [17] a detailed study has been performed, concerning the effect of total Nitrogen and PGS on intermediate Slab Reheating Temperature (1250°C), using HiB composition [19]. Its main results are hereby compared with MOGOCA-EVO Simulations.
Fig.14a shows the dependency of B8 against Nitrogen content for different decarburization temperature (chemical composition of the steel used is reported inside the graph, thickness is 0.285 cm). Moreover, Fig 14b also shows measured grain size after increasing decarburization temperature. The first observation is that PGS is rather small and only slightly bigger than that of HIB type. Moreover, B8 tends to improve as the grain size increases (max values reported in Fig.14c) and such optimization occurs at around 150 ppm of Nitrogen.
For the larger grain size (decarb. temperature) reported, a kind of unstable behavior seems to appear with a buildup of a double peak.
Increasing Nitrogen content, (85-300 ppm) there is an initial increase of B8 which reaches a stable zone around a maximum point, and then, according to the relative grain size, tends to decrease. The latter effect appears earlier and more significantly for smaller grain size.
It is worth stressing that this is the reason why HiB, which has PGS smaller than the smallest one reported in this study, cannot bear Nitriding to a level higher than 100-120 ppm without reducing B8 value. The fact that HiB can produce good B8 (values)

due to his extremely high inherent inhibition and small grain size is also linked to the remarkably high PGS microstructure homogeneity generated (HE=$R_{max}/R_{mean}$ < 2.0).

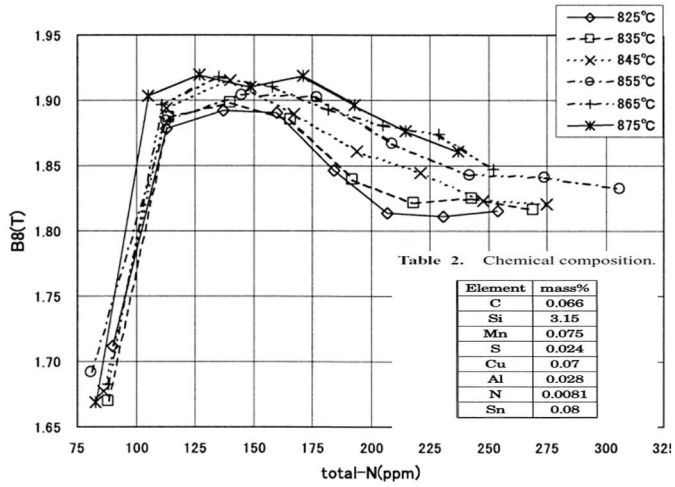


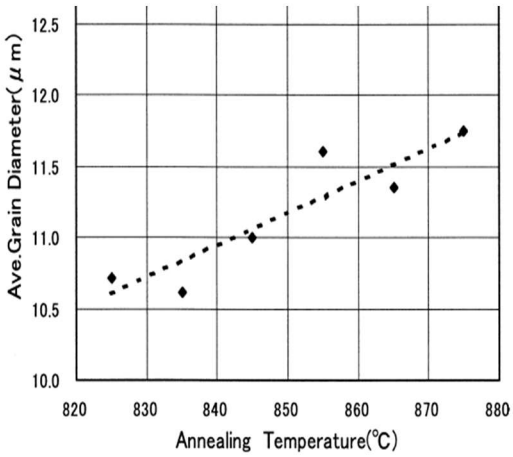


Fig.14a data from[19]

Fig.14b data from [19]

In Fig.15 simulations are shown using the same process parameters available from the paper. Intercept length is calculated from the 3-D grain radius (output of the Software) using ASTM-112 recommendations. Fig.14b assumes, based on our previous experiences, a heterogeneity factor of HE=2.2, as no information on the scattering of PRGS is available.

It is possible to see that all the effects previously discussed are very well described by MOGOCA-EVO, including an accurate reproduction of the double peak for the higher value of grain size, which means that it represents a physical effect and not due to experimental scattering, as it probably was assumed by the authors (which in fact didn't discuss it at all ).

Furthermore, the MOGOCA-EVO simulations (Fig.14d) confirm that the max value of B8 for each Decarburization temperature positively correlates with Grain size, as indicated in the same paper. However, Simulations in Fig. 16a show that such correlation, although weaker, is valid for larger GS as well.

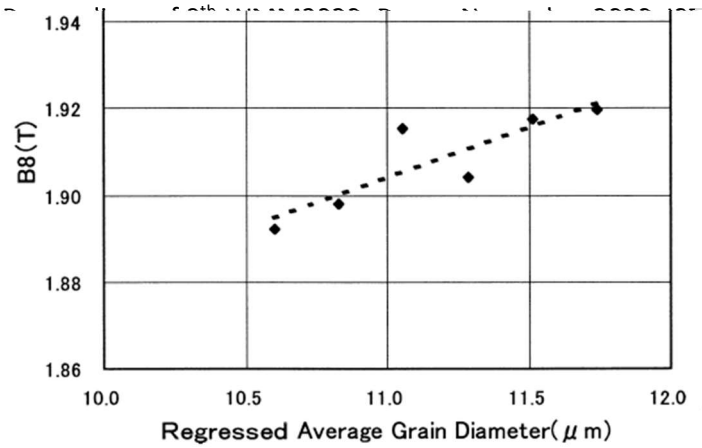


Fig.14c data from [19]

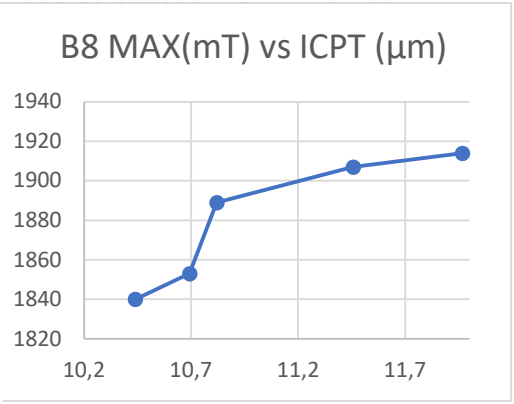


Fig.14d data from MOGOCA-EVO

Fig. 16b reports the Secondary Grain Size (SGS) as a function of Nitrogen content. The graph shows a tendency similar to that of B8 (Fig.15) with a maximum value in the range of 150-200 ppm, increasing as the PGS also increases. A set of macrographs for the secondary GS, associated to the experiments in Fig 14a , is reported In the paper by Kumano et al. [19]. Altough only qualitatively (no quantitative measurements are reported), the tendency shown in Fig. 16b is substantially confirmed.

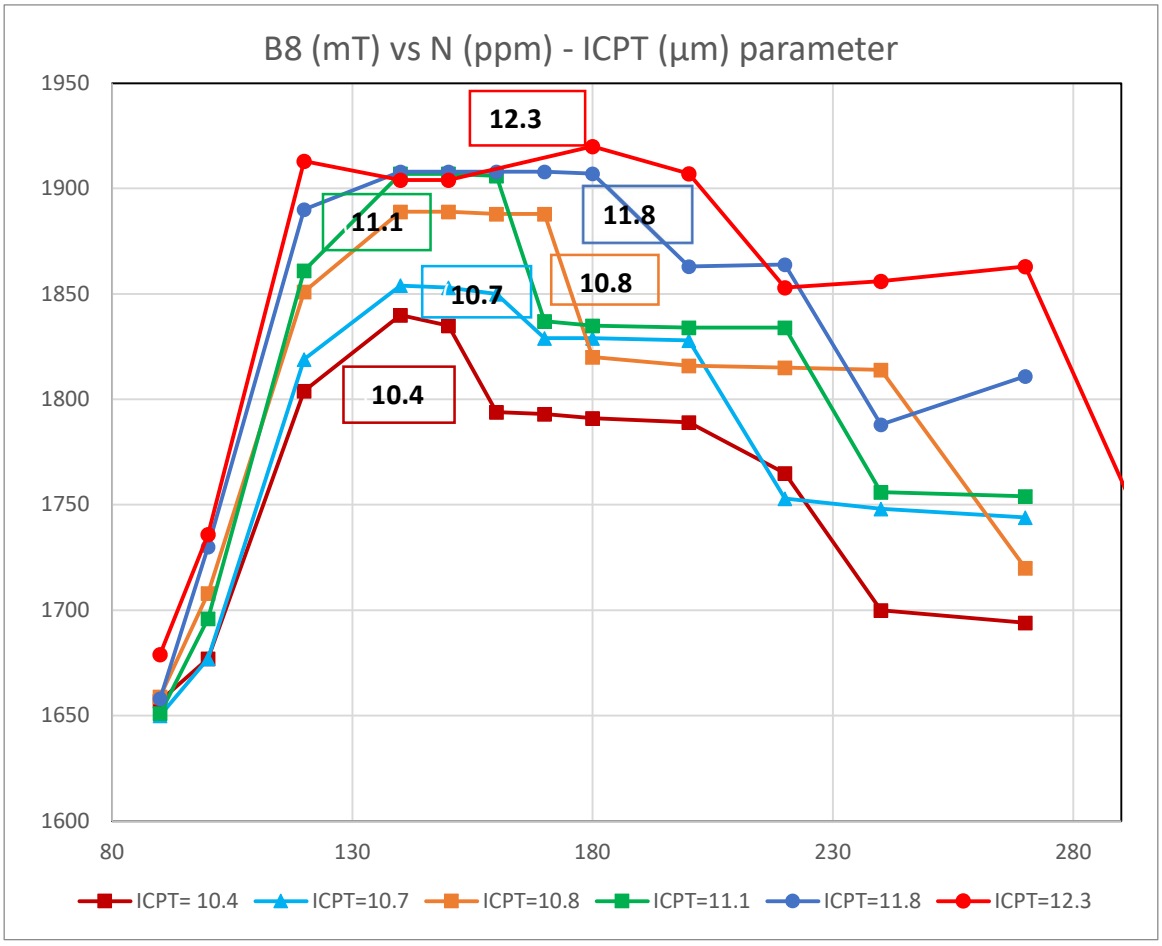


Fig.15 MOGOCA-EVO Simulations of case in Fig.14a

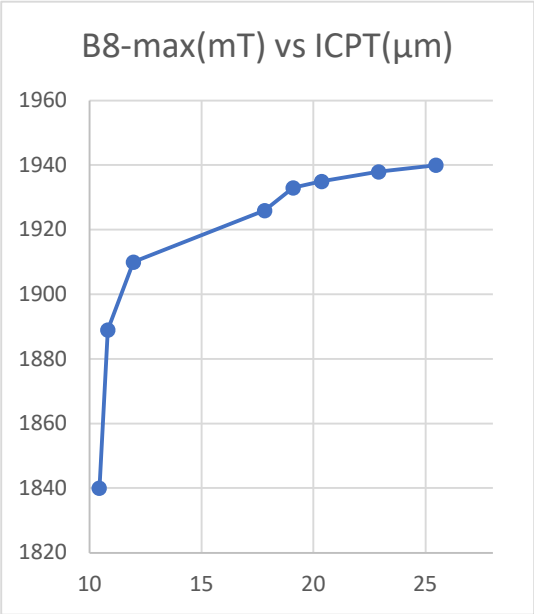


Fig 16a B8max vs PGS

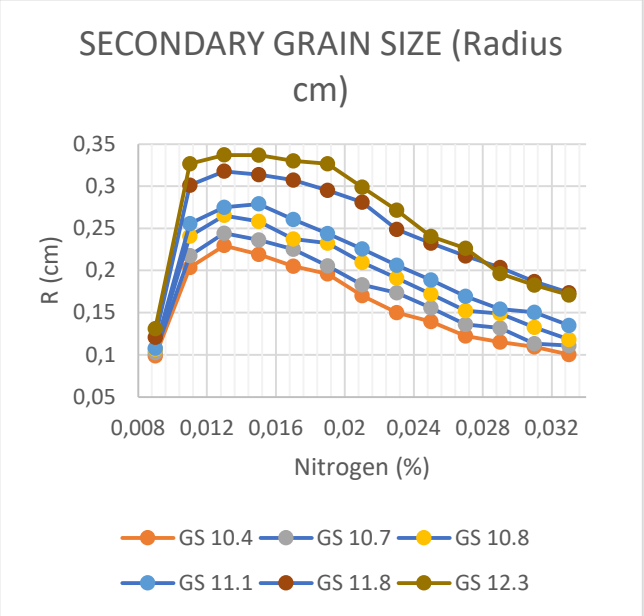


Fig.16b SGS vs Nitrogen (parameter PGS)

Moreover, performing simulations exploring PGS with the same heterogeneity factor adopted previously, one can see what occurs when increasing Nitrogen (90-330 ppm) , at least with the same conditions of chemical composition and process parameters adopted previously.
In fact, changing PGS we are roughly exploring the behavior of the various technology already mentioned (HTSR, ITSR-Thin Slab and LTSR) which are characterized by specific ranges of it.
Fig.17 features Simulations where the effect of Nitrogen, with PGS as a parameter (namely corresponding to the adopted technologies), influences B8. As it is possible to see, as Nitrogen changes (90-330 ppm) there is a B8 increase for each PRGS up to a maximum, which occurs, in the range between 180-220 ppm for PRGS 16-20 micron ,and in the range between 220-250 ppm for PRGS 20-23 micron, confirming the difference between intermediate inherent inhibition (as for instance Thin Slab technology) and LSRT, with low inherent inhibition.

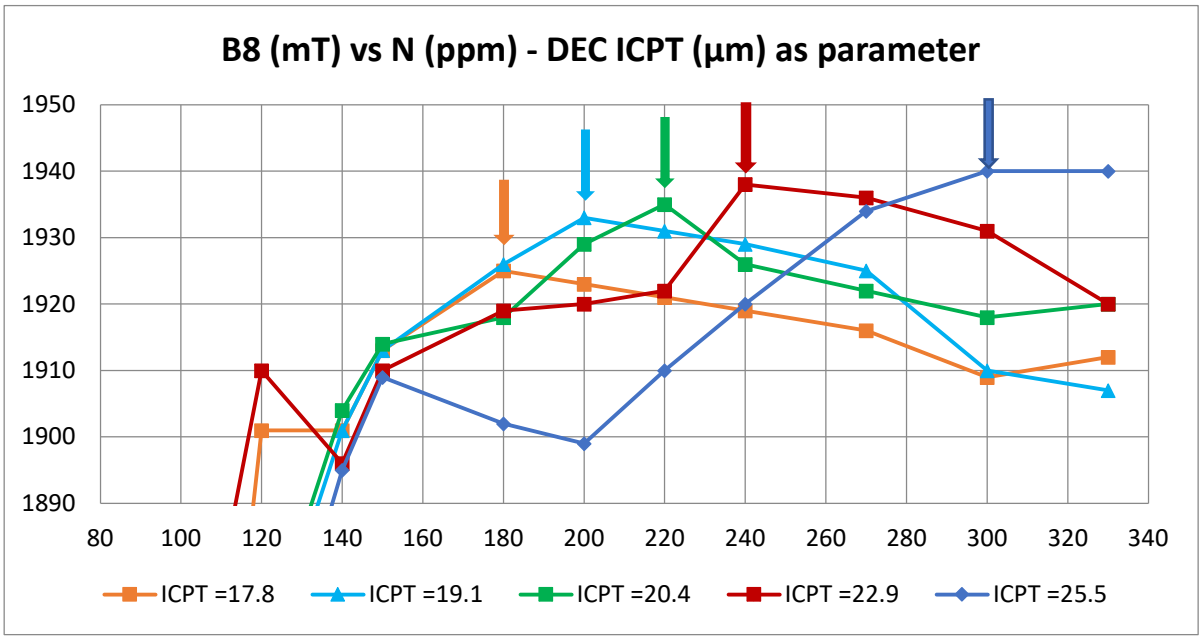


Fig.17 B8 vs Nitrogen with PGS as parameter

SGS as well (see Fig.18 ) shows a maximum associated with the same Nitrogen content which provides the best B8 value, confirming that optimization of Nitrogen content makes for a more refined selection of optimal Goss grains from the general Goss texture component.

Therefore, it is confirmed, as suggested by industrial evidence, that there is an optimization of Nitrogen content according to inherent inhibition and by consequence according to PGS and its heterogeneity, which strictly depend on it.

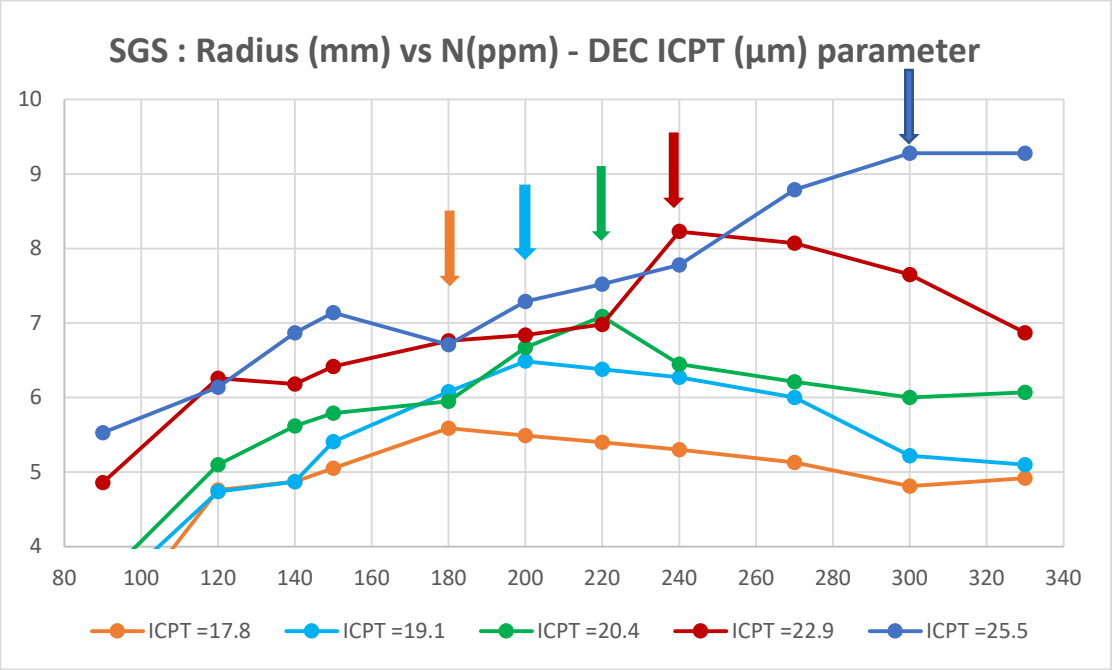


Fig.18 SGS vs Nitrogen with PGS as parameter

Let us now focus on the metallurgical background of such a Nitrogen effect, looking into the evolution of grain growth Inhibition strength during HTCA process.
As already established, and widely discussed elsewhere [1], MOGOCA Software can predict the evolution of the inhibition strength Iz during HTCA (see also fig.1b above). A set of Iz curves is thus shown in fig.19, for the case already discussed [19] , and for Nitrogen variable between 120 and 330 ppm.
As it is possible to see a bunch of intersecting curves are generated with a crossing point, common to all the lines with Nitrogen above or equal to 150 ppm, near which the inhibition's tendency to decay inverts the rate of change from low slope (for high Nitrogen) and high slope (for low Nitrogen) to the exact opposite, persisting for a significant interval of temperature. After that some of these curves (specifically the ones with high Nitrogen revert again the behavior until the fast drop of inhibition start at 1/5 of the thickness).
The only curve represented only for sake of clarity, which differs from the others is the curve for 120 ppm N (in particular with N under-stoichiometric with Aluminum content). Such curve shows a continuous and smooth drop until the unavoidable discontinuity of the slope at 1/5 thickness.
Since the typical temperatures of SRX start for HIB technology is in the 990-1010 °C range, this well explains why 120 ppm (or slightly less) of Nitrogen can work properly without experiencing the inhibition's fast drop there associated, which is definitely deleterious for selection of Goss grains. Moreover the typical temperatures of start SRX for Thin Slab are in the 1040- 1080° C range , while for LSRT they are between 1070- 1100° C or even higher (this can be also seen in the graphs of starting SRX temperature, which will be discussed in detail elsewhere[18]). In the range of temperatures just mentioned, the curves which have the smoother drop behavior are in fact exactly the ones around 200 ppm for TS and those around 240 ppm for LSRT.

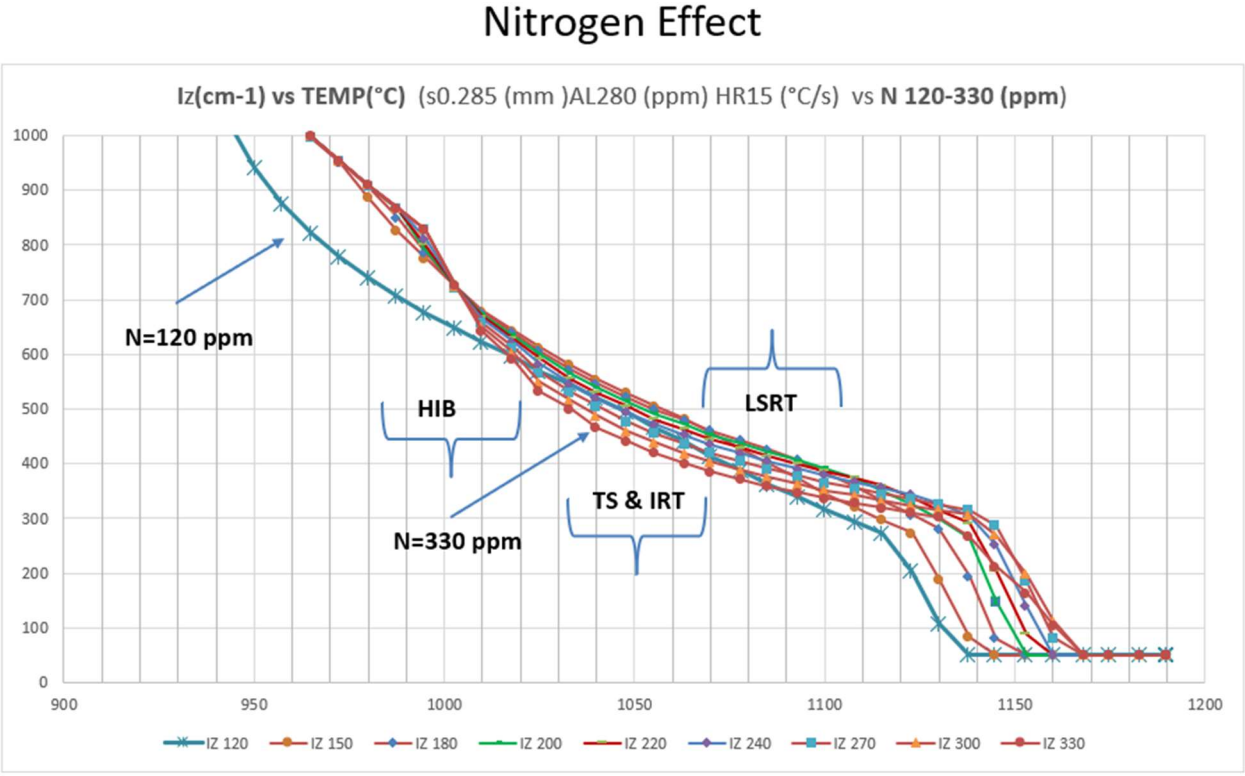


Fig.19 Inhibition strenght evolution vs Temperature with Nitrogen content as a parameter

# 8. Potential of MOGOCA-EVO for practical application

For the sake of brevity the large amount of details generated by the Software associated with the simulation will not be discussed in this article, each of which can shed light on the relevant parameters affecting the final results.
As a further example of a pratical tool that can be generated to analyze and optimize the practical results of the specific technology adopted, a two dimensional Magnetic MAP is shown below in which B8 is plotted as a function of Total Nitrogen and Primary Grain size. The details of the simulation are not reported but are in the typical range used for HGO process.The colors in the MAP represent in short homogeneous zones of B8 results and can be read as follows: dark red=unacceptable, red=bad, orange=insufficient, light greens=sufficient, dark green=good, blue=very good

One can produce a series of these Maps alternating the various parameters on the axis among those relevant for the final results and which are, case by case, object of optimization. In fact the parameters are many, as also reported in short in tables 1,2 in the APPENDIX, and the real integral plot would be a multidimensional plot as the one sketched in Fig.20 where the various axes (representing one parameter each) will give their contribution to refine the optimization area.

**Magnetic Map (B800)** by metallurgical and Process Parameters : 0.285 mm thick, Si=XX%, Al=XXX ppm, LOI=XX%,, Heating Rate=XX°C/h ; Standard Dec Oxide structure,.....

| ICPT (µm) | 12.7 | 15.3 | 17.8 | 19.1 | 20.4 | 22.9 | 24.2 | 25.5 | 26.7 | 28.0 | NITROGEN (ppm) |
|---|---|---|---|---|---|---|---|---|---|---|---|
| | 1662 | 1691 | 1737 | 1762 | 1764 | 1817 | 1817 | 1828 | 1794 | 1738 | 90 |
| | 1903 | 1910 | 1901 | 1864 | 1867 | 1910 | 1867 | 1854 | 1795 | 1751 | 120 |
| | 1909 | 1919 | 1901 | 1901 | 1904 | 1896 | 1905 | 1895 | 1876 | 1727 | 140 |
| | 1909 | 1919 | 1913 | 1913 | 1914 | 1910 | 1869 | 1909 | 1800 | 1701 | 150 |
| | 1909 | 1917 | 1925 | 1926 | 1918 | 1919 | 1917 | 1902 | 1781 | 1737 | 180 |
| | 1908 | 1918 | 1923 | 1933 | 1929 | 1920 | 1921 | 1899 | 1879 | 1695 | 200 |
| | 1867 | 1916 | 1921 | 1931 | 1935 | 1922 | 1923 | 1910 | 1845 | 1703 | 220 |
| | 1869 | 1914 | 1919 | 1929 | 1926 | 1938 | 1933 | 1920 | 1718 | 1719 | 240 |
| | 1816 | 1912 | 1916 | 1925 | 1922 | 1936 | 1940 | 1934 | 1730 | 1636 | 270 |
| | 1764 | 1853 | 1909 | 1910 | 1918 | 1931 | 1940 | 1940 | 1905 | 1715 | 300 |
| | 1719 | 1757 | 1912 | 1907 | 1920 | 1920 | 1930 | 1940 | 1925 | 1698 | 330 |

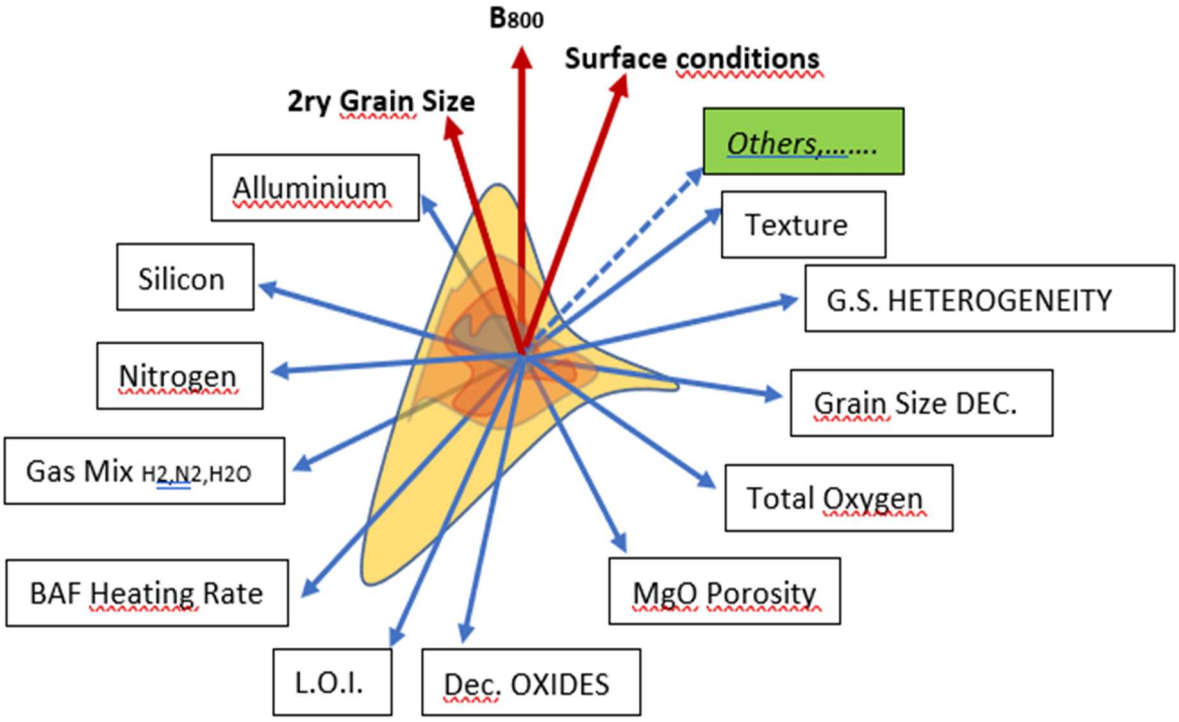


Fig.20- Hypersurface in a multidimensional Space. Identification of Optimization Area

Some of these parameters are directly operating on the HTCA process phase as they are inherent to the specific process conditions and chemical composition. Others act indirectly because of conditions generated in the Dec Line: by specific process conditions adopted in Dec Line (Thermal profile, gas atmosphere, MgO LOI,..) or

indirectly produced in the microstructure by the effects of previous process steps (going back to the casting and rolling conditions, treatment lines, warm rolling , inherent inhibition….)
This concept is outlined in the following diagram where the area of intervention of MOGOCA is singled out.

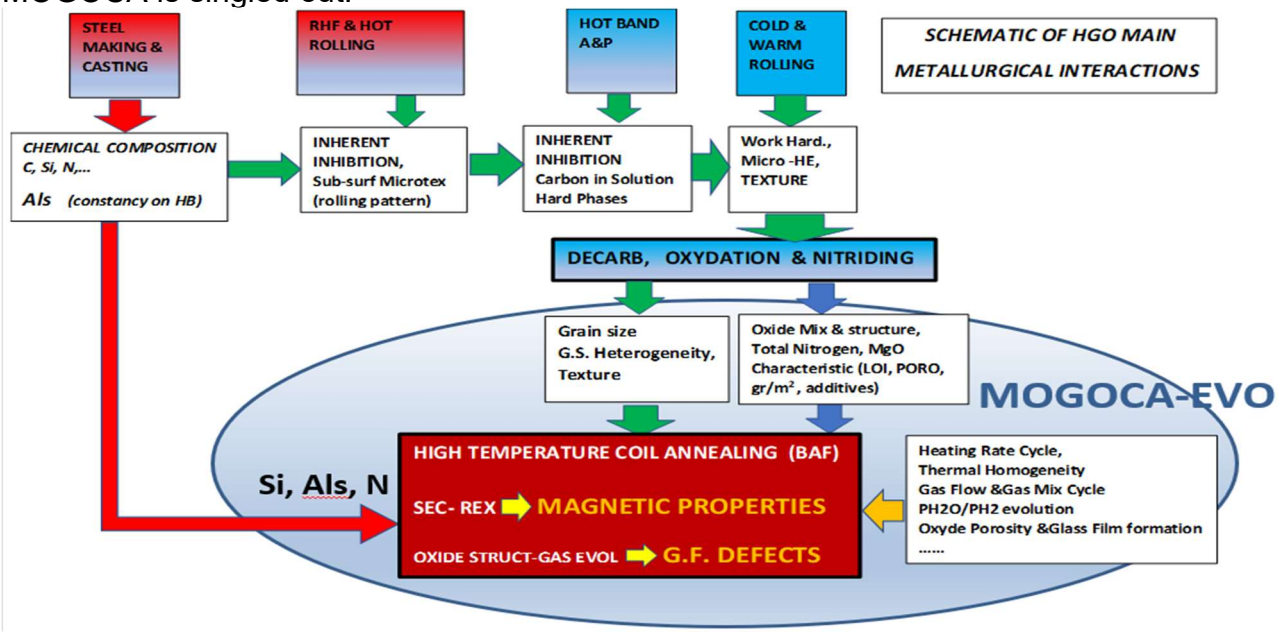


## 9. Conclusions

The general scope of such a Long lasting and Comprehensive Scientific Program was that to transform the GOES Production Technology as much as possible , from the typical **"Art " approach** (founded on extensive experience and continuous trial and error procedures) to a more **"Scientific" one** (Detailed Theoretical description with very specific associated experiments in case calibration is needed). Nowadays we have made great steps in the pursuit of this ambitious goal, which has almost been reached.

Such **breakthrough tool (MOGOCA & MOGOCA-EVO) is now capable of controlling the evolution of the microstructure** (precipitates, grain growth and texture) and predicting **Final Magnetic properties and Surface Quality** as a function of the numerous technical, microstructural and process parameters involved during the Final Coil Annealing, and also of those inherited by previous treatments, for example the Chemical Composition, hot and cold rolling and specific treatment lines (A/P and dec Lines).
MOGOCA-EVO shows that **the instability of the Magnetic properties** (B800) is strictly related, among other things, to the grain size after the decarburization step. The Software allows to single out and rank by significance the factors which influence such microstructure parameters, such as: Chemical composition, slab reheating and HR,

Hot band annealing & quenching, Cold & Warm Rolling and Decarb annealing conditions, ….
MOGOCA-EVO makes it easy to check all the **process parameters** that can create such instability and explain their specific **role in determining the final magnetic properties** (with the goal of improving the magnetic potential of the Product).

Such Advanced Software tool represents, **the more appropriate instrument for supporting and addressing all the Research efforts for the new expected developments (Products, Processes and Plants), as well as a practical tool for continuous Quality improvement and Production optimization.**
Ultimately, such basic and comprehensive approach provides **the natural Scientific and Technical environment in which to train and support Production Engineers, Quality experts and Researchers on the field of GO Technology**

***MOGOCA-EVO runs efficiently on a Laptop Computer****, allowing to perform fast scans on the influence of the various parameters which are being investigated. Such versatility and ease to use make it a practical tool for Industrial world.*

# 10. References

[1] G. Abbruzzese - Metallurgical model of high temperature coil annealing in GOES Production, Proc. WMM Dresden 12th - 14th June, 2018, ISBN 978-3-86012-579-3. Pages 630-649
[2] G. Abbruzzese, Acta Metall., 33, (1985), p.1329.
[3] G. Abbruzzese, S. Fortunati , J. Appl. Phys. 64 (10) 5344-5346 (1988)
[4] G. Abbruzzese and K.Lucke, Acta Metall. 34 (1986) 905
[5] G. Abbruzzese, K.Lucke and H. Eickeikraut, Trans ISIJ 28 (1988) 618
[6] G.Abbruzzese and A.Campopiano,J.Magn.Magn.Mater 133 (1994) 123
[7] G. Abbruzzese - SMM 16, Stahl und Eisen, Vol.1, pp.3-13 (2003)
[8] G.Abbruzzese and A.Campopiano, Recrystallization ’90, Wollongong The Metallurgical Society, (1990), 667
[9] Ibe G. and Lücke K., Recrystallization Grain Growth and Texture, ASM, (1966), p. 437.
[10] N.Takahashi and J.Harase, Mater.Sci.Forum 204-206 (1996) 143
[11] Y.Yoshitomi et al, Mater.Sci.Forum 204-206 (1996) 629
[12] Y.Ushigami et al., Mater.Sci.Forum 204-206 (1996) 593
[13] Hutchinson W.B. and Homma H., Grain Growth in Polycrystalline Materials III, (1998), p. 387.
[14] Y. Ushigami, T. Nakayama, Y. Suga, N. Takahashi, Mater. Sci. Forum, 204-206 (1996), pp. 605-610
[15] Y. Yoshitomi, K. Iwayama, T. Nagashima, J. Harase, N. Takahashi, Acta Met, 41, 5, 204-206 (1993), pp. 1577-1585
[16] Harase J. and Shimizu R., Acta Metall., 37, (1989), p. 1241.
[17] S. Cicalè, S. Fortunati, G. Abbruzzese S. Matera –Grain Growth in Polycrystalline Materials III Proceedings ICGG-3 Pittsburgh, Ed by H.Weiland, B.L. Adams, T. Rollet, The Mineral, Metals & Materials Society, Warrandale p.587 (1998).
[18] G. Abbruzzese et al., to be published
[19] T. Kumano, T. Haratani, N. Fujii, ISIJ International, vol.45, (2005) N°1, pp.95-100

# 11. APPENDIX

BASIC CHART OF MOGOCA SOFTWARE PACKAGE- STRUCTURE AND POTENTIAL - OF THE

***METALLURGICAL MODEL OF GRAIN-ORIENTED HIGH TEMPERATURE COIL ANNEALING*** (**M**OGOCA)

**Tab.1**

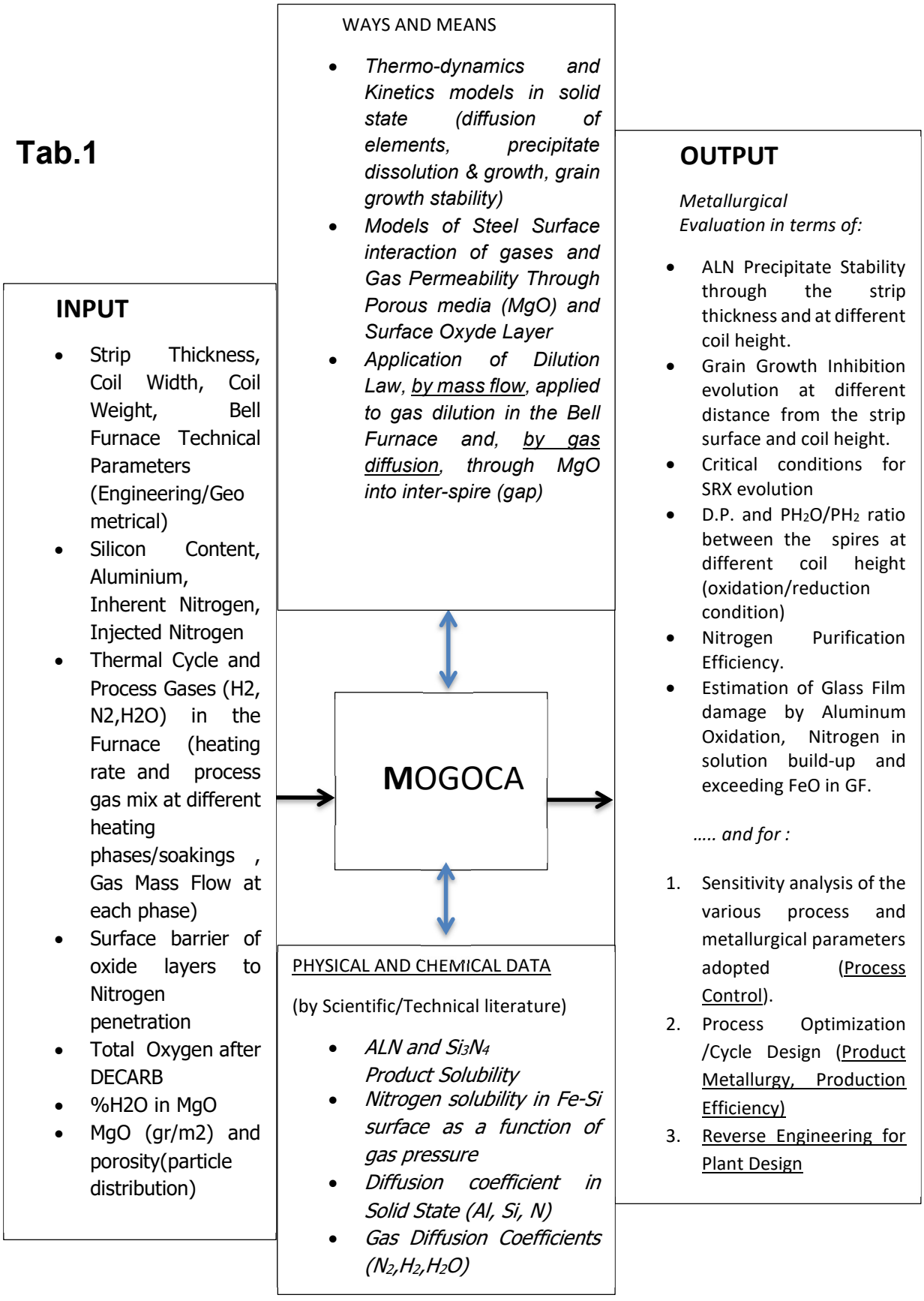

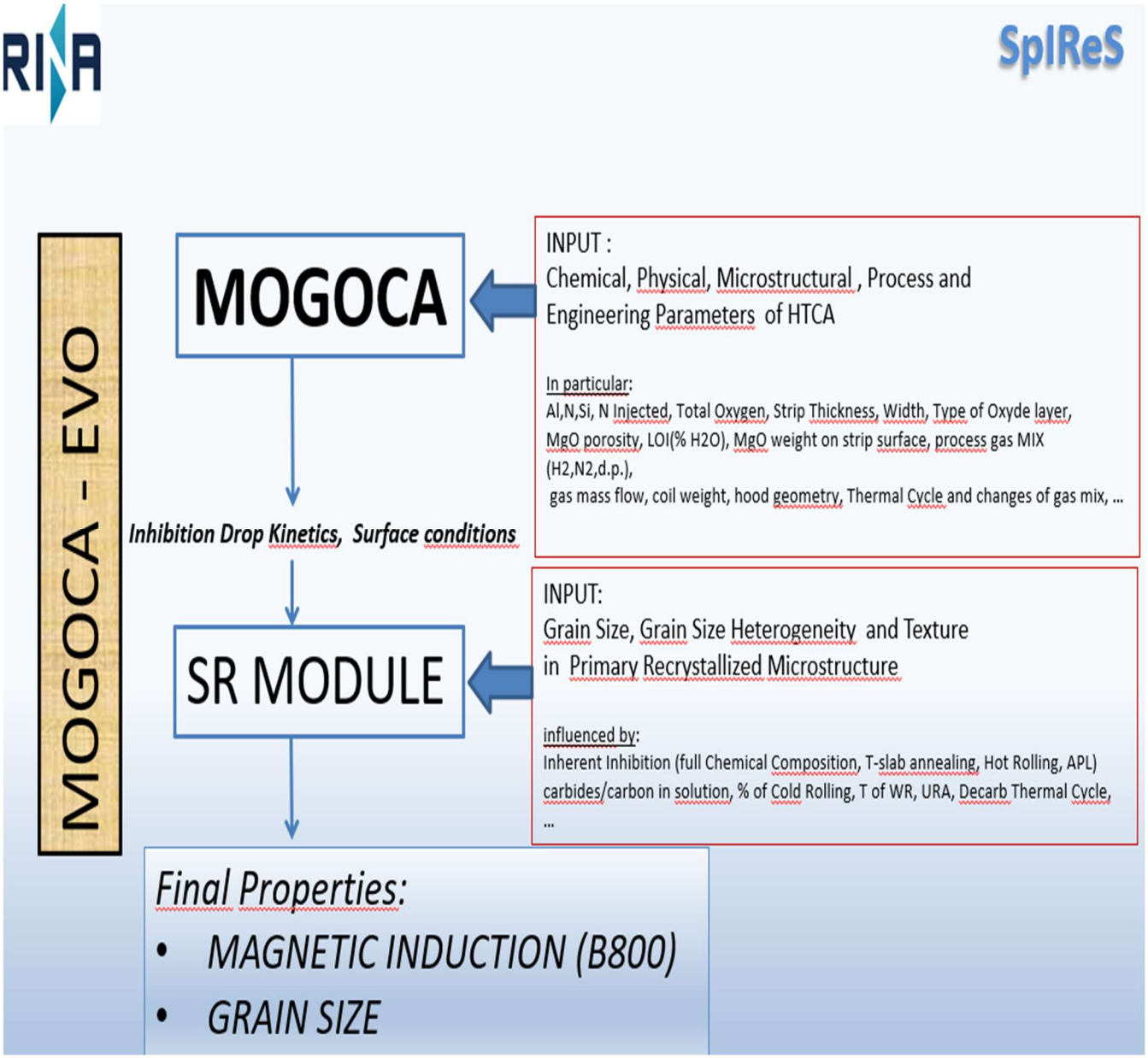


**Tab. 2**

## ACKNOWLEGMENTS

The Author would like to thank Mr. Simone Abbruzzese for his valuable support on data elaboration and paper preparation. The Author would also like to thank RINA-Consulting-CSM for its support in promotion and its role in commercialization of the **M**OGOCA- EVO Software